RESEARCH PAPER

Phytochemical Profiling and Molecular Docking Analysis of Diospyros malabarica Phytoconstituents against Bone Morphogenetic Proteins

Tamilselvi S. [1*], Sanjeevkumar S.S. [1], Anjali G.V [1], , Saravana kumar N.M [2], Mithra R[1],Prabavathi S[1], Mahima R[1], Kavin S[1],

[1.] Department of Biotechnology, Bannari Amman Institute of Technology, Sathyamangalam – 638401, Tamil Nadu, India.

[2.] Department of Computer Science and Engineering, Sri Shakthi Institute of Engineering and Technology, Coimbatore - 641 062, Tamil Nadu, India.

Corresponding author: Dr.S.Tamilselvi

tamilselvis@bitsathy.ac.in

ABSTRACT

Osteopathic disorders such as osteoarthritis and skeletal injuries require novel bioactive therapeutics. Diospyros malabarica, traditionally used for bone setting, was investigated for its osteogenic potential. Soxhlet extraction using n-hexane, methanol, and water showed the highest yield in methanol extract (2.49 g/30 g). GC–MS analysis identified 204 compounds in methanol and 357 in n-hexane extracts. FTIR and NMR analyses confirmed the presence of bioactive phytoconstituents. Compounds such as lupeol, erucic acid, palmitoleic acid, and silane trichlorodocosyl were identified as potential osteogenic agents. Molecular docking against BMP-2, BMP-4, BMP-6, BMP-7, and BMP-9 proteins revealed lupeol exhibited the strongest binding affinity with BMP-6 (–9.2 kcal/mol), supporting the traditional therapeutic relevance of D. malabarica in bone regeneration.

Keywords: *Diospyros malabarica*, phytochemical analysis, Osteogenesis, Bone regeneration, Bone Morphogenetic Protein, Molecular docking.

How to cite this article: Tamilselvi S. Sanjeevkumar S.S. Anjali G.V Saravana kumar N.M Mithra R,Prabavathi S, Mahima R, Kavin S,. Phytochemical Profiling and Molecular Docking Analysis of Diospyros malabarica Phytoconstituents against Bone Morphogenetic Proteins. Int J Drug Deliv Technol. 2026;16(79s):684-686. DOI: 10.25258/ijddt.16.79s.129.

INTRODUCTION

Diospyros Malabarica, belonging to the Ebenaceae family, is an indigenous species of India. Its biodiversity has been reported widely in Western Ghats most prevalent in the Pothigai malai hills of Tirunelveli also in Karnataka, Maharashtra, Assam, Nepal, Bangladesh, Lahore in Pakistan and Norther provinces of Sri Lanka (Figure 1) [1–8]. Commonly named as Pannacai, Pallingi kai in Tamil; Gaub, Tinduka, and Tinduki in Sanskrit as Indian persimmon [9]. Fruits, leaves, bark of this plant were used in the multiple traditional formulation of Ayurveda and Siddha medicine attributing to its antioxidant, anti-microbial, anti-inflammatory, anti-diabetic, anti-cancer, anti-diarrheal, anti-coagulative, anti-helminthic neuropharmacological and analgesic activities[2,7,10–15] Even though properties of several parts of this plant were investigated ,the unripen fruit is still not scientifically explored, as it is found to be used in the traditional formulation of bone setting, fractures and osteoarthritis [1], but these activities were not studied tends to target on bone regeneration parameters. In addition, the phytoconstituents of the fruit was not reported clearly in previous studies, therefore profiling the phytoconstituents will also help to understand the role and their involvement in bone regeneration along with their pharmacological activities.

Bone healing and regeneration process recruits immune cells and release cytokines to initiate angiogenesis and MSC's proliferation as acute inflammatory process, to prevent this acute inflammation to turn into chronic inflammation anti-inflammatory cytokines are released to balance and resolve the inflammation at the site simultaneously to initiate the osteoblast proliferation [16]. Polyphenols, Terpenoids, alkaloids and essential oils are phytochemicals with anti-inflammatory activity tend to modulate the signaling pathways directly or indirectly to reduce the inflammation phase [17]. Similarly, GC-MS studies of *Diospyros* species showcased abundance of phenols, alkanes and terpenoids [18] compounds due to fruits of *Diospyros malabarica* may also have these compounds, making it potential alternative anti-inflammatory agents as alternatives for current NSAIDs. Bone is an integral skeletal organ providing structural and mechanical support for joints, tendons, and ligaments. It regenerates and mineralizes the tissue matrix regularly at adequate levels, to maintain a healthy bone because bone is involved in various crucial processes of our body, such as mineral homoeostasis, immune and hormonal regulation [19]. Bone tissue matrix is composed of 90%

type I collagen, 10% non-collagenous protein like osteocalcin, osteonectin, bone sialoproteins and proteoglycans contributing to matrix maturation, mineralization and osteoblasts and osteoclasts as bone cells along with their precursor & associated cells, are organized as bone multicellular units [20].

The main function of this unit is to mediate bone rejuvenation/remodel osteo-integrity during bone development and regeneration during fracture healing, Abnormal or poor bone development would lead to multiple conditions osteoporosis, osteogenesis imperfecta, Paget's disease, etc. [19].

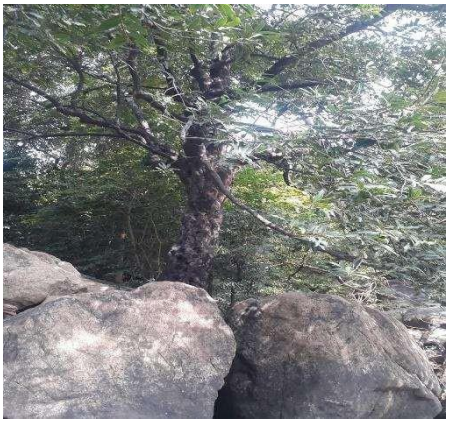

Fig 1.a – *Diospyros malabarica* fruit, 1.b. – *Diospyros malabarica* tree, 1.c – geographical tag of sample collection site

Bone regeneration is a complex physiological process that spans from embryonic development to continuous remodeling throughout adult life as well as a repair process during injury and fractures. The process takes place with the series from bone induction to conduction involving numerous cell types, cellular & molecular signaling pathways. During embryonic skeletal development the flat bones are developed by differentiating Mesenchymal stem cells directly into bone cells known as intramembranous ossification, at the same time long bone are developed through endochondral ossification depending on the cartilage formation. Subsequently invaded by osteoprogenitor cells of vascular tissue, later removed and replaced by bone cells for ossification in the middle and at the ends of the developing bone. Post-embryonic stage i.e. bone during adult life undergoes a regular remodeling process through a balanced cyclic process of osteoclasts and osteoblasts formation regulated by RANKL pathway for osteoclast activation, Bone morphogenetic proteins (BMPs) and Wnt signaling pathway promotes osteoblast differentiation, even though osteoblast, osteoclast and osteocytes have separate activity but they are closely linked with few coupling factors such as TGF-β, ephrin - B2, B4, semaphorin 4D. In this overall process, if the bone mineralization or remodeling happens poorly will lead to fragile bones having higher chances of fracture due to low shock-absorbing strength [19].

Bone fractures are referred to as detachment or bone discontinuity depending on the severity and the region of fractures. Direct healing (primary) and indirect healing (secondary) includes a combined process of hematopoietic and immunological cells [21]. Primary healing occurs only when bone fragments are reduced, aligned and fixed under a compression state without any motion in such a way that one side of the cortex must connect to the other side to reestablish mechanical and physical continuity. At the site of fracture, cutting cones are formed at the end of osteons. These cones cross the fracture lines and generate longitudinal activities through osteoclasts and osteoblasts, by generating a bone matrix that allows blood supply supporting bone reestablishment. At the end osteons mature and undergoes remodeling. Primary healing is most observed in lamellar bone and heals the fracture site without callus formation and inflammation [22]. Secondary healing is the most common way of fracture healing, consisting of intramembranous and endochondral ossification, like embryonic bone formation, with four stages of healing. The 4 stages of bone formation are (i) Acute inflammatory response or hematoma formation (ii) differentiation and proliferative phase (iii) callus formation phase (iv) bone remodeling phase. When a bone tissue undergoes a fracture, it immediately initiates with hematoma formation as acute inflammatory response, in this hematoma coagulates to form temporary scaffold that acts as template for callus formation involved with recruitment of inflammatory markers such as TNF-α, IL – 1, IL-6 then attract the macrophages, lymphocytes, monocytes to remove necrotic tissue and secretes the cytokines such as vascular endothelial growth factor to stimulate healing by promoting angiogenesis, this phase last for 5 days. The 2nd involves the

differentiation and proliferation of cells to form a fibrocartilaginous network by differentiating fibroblasts, osteoblast, and chondroblasts from the mesenchymal stem cells, initiating the deposition of collagen-rich fibrocartilaginous network through chondrogenesis along with a layer of woven bone as this takes place for another 5 days. The 3rd stage takes up to 4 weeks with multiple overlaps with previous phase as it is involved in the bony callus formation, were cartilaginous callus (soft callus) is ossified through endo chronal ossification to form a hard callus (via chondroblast, osteoblasts and osteoclasts) as part of last stage it undergoes remodeling of bone to form a compact bone centrally and lamellar bone peripherally to achieve the rigidity and biomechanical stability as like normal bone similarly this the longest phase among all as it can last from months to years [23].

The overall bone formation, regeneration and fracture healing is carried out through cellular signaling pathways such as RANKL/OPG pathway, Wnt signaling pathway, Notch and BMP's regulated with few growth factors i.e. cytokines, hormones. The mechanism of many growth factors such as BMPs, TGF-β, FGF, PDGF and IGF at extracellular levels until gene transcription reported to be directly involved in bone formation. Amongst all signaling pathways BMP/ TGF-β contributes majorly responsible for the bone forming cellular process, disruption in this pathway will lead to multiple disorder and osteoarthritis [24].

BMP are multifunctional cytokines, synthesized as active large pre-pro-polypeptides with signaling peptides at their amino terminal and mature polypeptides at the carboxyl terminal which is separated by pro-domains. The precursor protein is cleaved by furin, a pro-protein convertase to liberate mature BMP polypeptides, the monomer of mature BMP contains 7 cysteines, in which 6 form an intramolecular disulfide bond and the 7th residue is involved in dimerization with another BMP through covalent disulfide bond resulting a capable ligand for BMP receptor activation. BMP homodimers are well characterized both in-vivo and in-vitro whereas few heterodimers such as BMP-2/5, 2/6, 2/7, 4/7 demonstrate an enhanced activity in mesoderm induction and bone marrow cell differentiation. Crystal structure of BMP homodimers consists of cystine-knot with characteristics of "wrist and knuckle" or "two bananas" shapes, structural analyses further identified key receptor and antagonist binding sites for studying the BMP receptor interaction and regulatory mechanism [25].

BMP belongs to TGF-β superfamily and overall, 20 BMPs is identified in which BMP-1, is a procollagen C proteinase with 730 amino acids with cysteine rich residue, remaining BMP are classified into 4 sub-families such as TGF-β sub family, BMP sub family, growth and differentiation factors (GDFs) subfamily and subfamily of activins/ inhibin, similarly based on the homology this is generally classified into 4 categories of BMP – 2/4; BMP-5/6/7/8a/8b; BMP – 9/10 and BMP 12/13/14. The BMP receptors are serine/threonine kinase receptor are of two subfamilies, type – I and type II, type I consists of 5 BMPR such as ALK 1(Acvrl 1), ALK2 (ActRI), ALK3 (BRIa),

ALK4(ActRI), ALK6 (BRIb) and type II consists of 3 BMPR such as BRII, ActRIIa and ActRIIb. BMP signals are signaled in two pathways the classical Smads-dependent pathway and non-classical Smads independent mitogen activated protein kinase pathway. In classical pathway BMP binds to type I and II receptors and phosphorylated through Regulator Smads (R-Smad) i.e. Smad-1,5,8 and forms a complex through Smad 4 i.e. Co-mediated Smads (Co-Smad) then translocated into nucleus to regulate gene-transcription to promote osteoblast differentiation. Similarly in MAPK pathway signal pathway transduce into nuclei via JNK-1 and 2/3, ERK1/2, NF-B and p38 to regulate the genetic expression of their role [26].

There are almost 20 Bone morphogenetic proteins, expresses or involved in various process such ways BMP-2, BMP-3, BMP-4, BMP-6, BMP-7, BMP-9 are most observed in the bone formation and fracture healing process. BMP 2, acidic glycoprotein regulates the Smad Signaling pathway to activates the osteoid, deficiency of BMP-2 will impair osteoprogenitor cell differentiation leads to abnormal healing and tissue imbalance. A secretory protein called BMP-4 is like BMP-2 with 83% homology regulates osteoclastogenesis by stimulating the p38 MAPK pathway, also co-operates with VEGF to enhance MSC recruitment during fracture repair. In addition, BMP-6 glycoprotein has properties to promotes the extracellular mineralization as well as induce the alkaline phosphatase activity to enhance osteoblast differentiation from MSC also it has comparatively a rapid osteogenic induction from BMP-2. Similarly, BMP-7 as like BMP-2 stimulates the collagen synthesis, deposition of calcium and mineralization. Unlike other BMP's BMP –9 (GDF-2) promotes an effective bone formation than BMP 2/7 as well as responsible for bone rigidity similarly it activates Smad- 1/5/8; p38 and ERK 1 / 2 in MSC via ALK 1 and 2 signals. Apart from this BMPs, BMP – 3, BMP-12 induces cartilage, tendons and ligament formation

2.2.2. Phytochemical Characterization studies

The phytochemical characterization studies investigated the presence of phytoconstituents in the sample *Diospyros malabarica.* Profiling the phytoconstituents aids in understanding their nature, which indirectly supports the bone formation and fracture healing [27].

Molecular docking is a computational method used to study the binding interaction between the targeted protein and ligand molecules. This study gives us a better understanding of the most effective binding site of the targeted protein. Through binding affinity, we can interpret how effectively the target protein express its role with and without the ligand molecules [28] .Similarly, the present study aimed to evaluate the

fracture-healing potential of phytoconstituents derived from Diospyros malabarica by targeting BMP proteins associated with osteogenesis and bone repair.

Molecular docking analysis provided insights into protein–ligand interactions, where binding affinity and docking scores served as indicators of phytoconstituent efficacy and their potential role in promoting bone formation and fracture healing.

2. Materials and Methods

2.1. Plant sample collection and authentication

Unripe fruits (500 g) of Diospyros malabarica were collected from the forest regions of Agasthiar Falls (8°42′14.23″N, 77°21′49.07″E) during January 2023. Plant material was authenticated at the Botanical Survey of India, TNAU campus, Coimbatore (Authentication ID: BSI/SRC/5/23/2022/Tech).

Samples were surface sterilized, sliced, shade dried at room temperature for 3 days, and pulverized into fine powder for further analysis.

2.2. Materials and Methods

2.2.1 Phytochemical Extraction

Phytochemical extraction of powdered unripe fruits of Diospyros malabarica was performed using distilled water, methanol, and n-hexane through Soxhlet extraction based on solvent polarity and compound solubility. Briefly, 30 g of powdered sample was extracted with 300 mL of respective solvents under optimized extraction cycles at their corresponding boiling temperatures. The obtained crude extracts were concentrated to 10 mL using a rotary evaporator to remove excess solvent and subsequently stored under refrigerated conditions for further analysis. Extraction yield (%) was calculated using the standard gravimetric formula.

$$Percentage\ yield = \frac{weight\ of\ extract}{weight\ of\ dried\ sample\ powder} \times 100$$

Equation 1: Percentage Yield of phytochemicals crude

role of their expression activity for pharmacological studies

2.2.3. FTIR

1ml crude extract of methanol, n-Hexane and distilled water was analyzed using Nicolet iS50 model in an

ATR mode with a wavelength ranging from 500 cm-1 to 3500cm-1.

2.2.4. GC-MS

GC–MS analysis of methanol and n-hexane extracts from unripe fruits of Diospyros malabarica was performed using a Clarus 680 GC-MS equipped with an Elite-5MS fused silica capillary column (30 m × 0.25 mm × 250 μm). Helium was used as the carrier gas at a constant flow rate of 1 mL/min. The oven temperature was programmed from 60°C to 300°C at 10°C/min and maintained for 6 min. Mass spectra were acquired under electron impact ionization at 70 eV within a scan range of 40–600 Da. Phytoconstituents were identified by comparison with the NIST 2008 spectral library.

2.2.5. NMR

The crude extract of *Diospyros malabrica* dried under reduced pressure was dissolved in two different solvents (methanol and water). NMR spectra were analysed under room temperature using a Bruker AVANCE III 500 MHz NMR Spectrometer. 32 scans of proton NMR spectra was acquired along with pulse sequence of proton decoupled. Carbon 13 NMR spectra was obtained using scans under appropriate pulse sequence. Relative to residual solvent peak chemical shift were recorded in parts per million.

2.3. Computational studies

Computational studies help to investigate, screen the phytoconstituents with various parameters computationally

2.3.1. ADMET Properties

ADMET profiling of phytoconstituents identified from *Diospyros malabarica* was performed using SwissADME and pkCSM. Canonical SMILES of selected compounds were retrieved from PubChem and subjected to pharmacokinetic and toxicity prediction analyses. Key parameters evaluated included lipophilicity (Log P), water solubility (Log S), rotatable bonds, hydrogen bond donors and acceptors, gastrointestinal absorption, blood–brain barrier permeability, and toxicity indices such as AMES toxicity, hepatotoxicity, and skin irritation. Compounds satisfying acceptable drug-likeness and safety criteria were shortlisted for subsequent ligand preparation and molecular docking studies.

2.3.2. Protein retrieval and preparation

Protein targets were identified and retrieved in PDB file format from RCSB PDB database which are experimentally determined 3D structures. The crystal structures of BMP's were retrieved with a refinement of size less than 3Å and X ray - diffraction method for structural confirmation.

2.3.3. Ligand retrieval and preparation

Ligands are the signaling molecules involved in the various cellular process. Phytocompounds tested for ADMET parameters are chosen as ligand then the 3D structure of these filtered compounds are downloaded in Structural Data Format file from PubChem database and further converted into PDB file using discovery studio software.

2.3.4. Molecular docking

Molecular docking was performed using PyRx to evaluate protein–ligand interactions between selected phytoconstituents and osteogenic target proteins. Ligands and macromolecular targets were prepared and converted into PDBQT format prior to blind docking analysis. Grid mapping was

configured to encompass the entire protein surface to identify all potential binding sites. Docking simulations were conducted for 11 ligands against 5 target proteins, and binding affinities were calculated based on the lowest binding energy values. Docked complexes were visualized using BIOVIA Discovery Studio Visualizer.

Protein–ligand complexes were exported in PDB format, while binding affinity data were retrieved in CSV format. Complexes exhibiting the highest negative binding energies were considered to possess the strongest binding interactions.

2.3.4 Binding interaction visualization

The binding interaction can be visualized in a 2D structure using Discovery studio software. Discovery studio is visualization tool for studying the biological structure, similarly it illustrates the binding interaction between ligand and protein more specifically the active binding site

containing functional groups of amino acids. The complex structure of docked molecules was visualized in 2D structure expressing the type of interaction and interacting position of amino acids, later this visualization is designed as per requirement and is saved as PDB format

3. Results and Discussion

3.1 Phytochemical sample preparation

The Soxhlet cycles were optimized for each solvent and maximum solvent yield obtained was 250ml. The maximum crude yield was obtained from 19 cycles for methanol, distilled water and 8 cycles for n-hexane. The maximum yield of crude was obtained from methanol qualitatively but quantitatively based on the number and classes of phytocompounds n-hexane extract had the maximum efficiency, similarly all the further studies are performed with crude form of extract. The extraction yield percentage of the sample is detailed in **Table 1.**

Table 1: Extraction yield (%)

Solvent	Powdered mass	Extracted mass (ml)	Yield value (%)
Methanol	30g	250	6.5
n-Hexane	30g	250	5.49
Distilled water	30g	250	8.3

Due to resin like consistency, methanol extract at room temperature solidifies like crystal, making it difficult to dissolve in normal parameters, hence it should be stored in refrigerated condition. Based on the solvent nature distilled water and methanol extract ended up in red color, but the n-hexane extracted were extracted resulted in green color.

Previous studies performed the extraction of plant sample by macerating the residual samples after using solvent in order of petroleum ether, dichloromethane, ethanol, methanol, ethyl acetate and water for 72 hours with an extract yield ranging from 6.5 - 8.3% expressing a higher yield with distilled water [29,30].

3.2. Phytochemical characterization studies

3.2.1 FTIR

As FTIR is used to interpret the functional group present in the crude extract helps to predict the presence of different types of metabolites. The spectral position of graph showcases the suitable functional groups because functional group expresses itself only in few specific ranges. The methanolic extract expresses stretching's of N-H, C=C, C-F, the n-hexane extract expressed the stretching's of C-H, O-H, N-H, C=O and bend of C-H and the distilled water extract expressed the stretching's of alkene and amine. The FTIR spectrum for three different solvents analyzed (**fig 2.a, 2.b, 2.c.)** revealed the presence of functional group present in the bioactive compounds are listed in **Table 2**. [31,32]

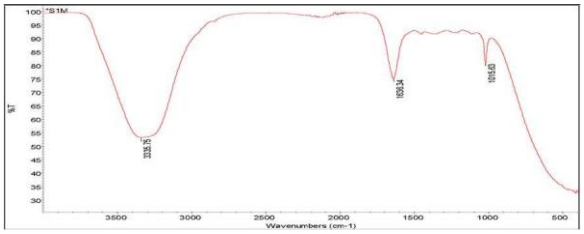

Fig 2.a: FTIR spectrum of methanol extract

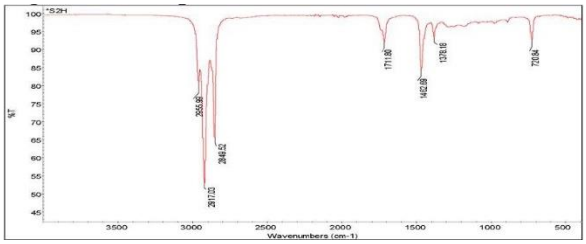

Fig 2.b: FTIR spectrum of n - Hexane extract

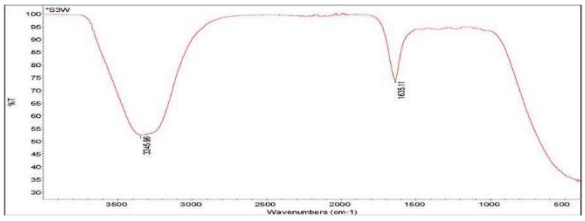

Fig 2.c: FTIR spectrum of distilled water extract

Table 2: Functional groups identified from FTIR analysis

Extract	Wavenumber (cm^{-1})	Functional group	Bond type
Methanol	3335.75	Amine	N–H stretching
	1636.34	Alkene	C=C stretching
	1015.63	Fluoro compounds	C–F
n-Hexane	2953.99	Alkane	C–H stretching
	2917.03	Amine	N–H stretching
	2849.52	Alkane	C–H stretching
		Amine	N–H stretching
	1711.80	Carboxylic acids, aliphatic ketone	C=O stretching
	1462.69	Alkane	C–H
	1378.18	Phenol, alcohol	O–H bending
	720.84	Benzene derivatives	C–H bending
		Alkene	C=C stretching
Distilled water	3345.96	Amine	N–H stretching
	1635.11	Alkene	C=C stretching
		Alcohol, carboxylic acid	O–H stretching

Table 3: Compounds identified in Methanol extract

Sr. No.	Retention time (min)	Compound name	Formula	Molecular weight	Area (%)
1	10.302	1,2,3-benzenetriol	C6H6O3	126	53.9
2	10.777	No Hits	—	—	13.56
3	16.804	DL-glyceraldehyde dimer	C6H12O6	180	3.04
4	16.969	DL-xylose	C5H10O5	150	16.61
5	17.125	DL-glyceraldehyde	C3H6O3	90	30.58
6	17.270	1-guanidino-2-propanol	C4H11ON 3	117	15.97
7	21.831	No Hits	—	—	2.69
8	25.208	4-methoxyazolidine	C4H9ON	87	3.09

3.2.2. GC-MS

GC–MS profiling of methanol and n-hexane extracts from unripe fruits of Diospyros malabarica identified diverse phytoconstituents based on retention time, peak area, and spectral similarity against the NIST library. Methanolic extract revealed major compounds including 1,2,3-benzenetriol, DL-glyceraldehyde dimer, DL-xylose, diglyceraldehyde, 1-guanidino-2-propanol, and 4-methyloxazolidine. The n-hexane extract exhibited a broader phytochemical profile comprising 9-hexadecenoic acid, nonadecane, silane trichlorodocosyl, trans-1-butyl-2-methylcyclopropane, di-n-octyl phthalate, dichloroacetic acid nonyl ester, carbonochloridic acid decyl ester, and Lupeol. Among the identified compounds, lupeol and silane trichlorodocosyl demonstrated notable abundance and potential biological relevance. Detailed spectral profiles and compound identification data are presented in Fig. 3a–b and Table 3.

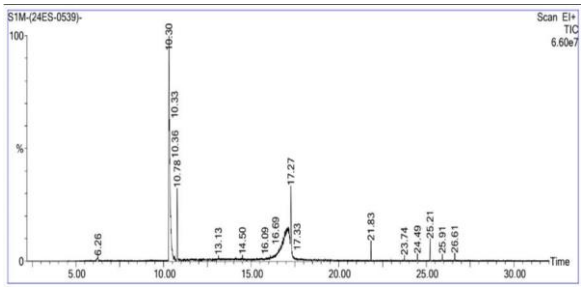

Fig 3.a. GC-MS spectrum of Methanol extract

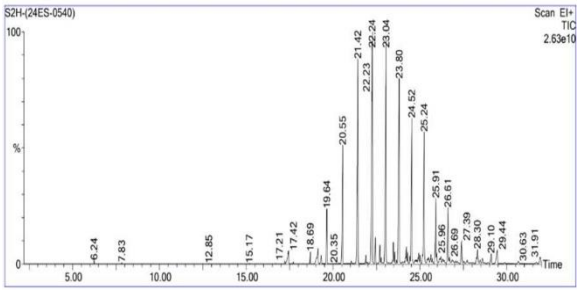

Fig 3.b. GC-MS spectrum of n-Hexane extract

3.2.3. NMR

The NMR analysis for solvents methanol and water exhibited lower number of scans, for both the samples due to low natural abundance and sensitivity. The wide spectral width of 24038 hertz and chemical shift range between 0 –200 ppm was noted, typical 13C NMR requires 100 – 1000 of scans whereas the results showed lower number of scans represents the lower visibility of compounds leading to improper peaks (Table 4).

The effectiveness of group identification hinges on the accurate correlation between structural groups and peak signals, because each group expresses itself at specific characteristics peaks in NMR spectra, but it has higher chances of overlapping especially in 13C NMR, then identified group are assigned by refining the linkages to distinct peaks even in mixtures. [33].

Table 4: Compounds identified in n-Hexane extract

Sr. No.	Retention time (min)	Molecule name	Formula	Molecular weight	Area (%)
1	17.435	No hits found	—	—	7.85
2	19.120	9-Hexadecenoic acid	C18H34O	266	8.09
3	19.635	Tetradecane, 1-iodo-	C14H29I	324	15.32
4	20.546	Nonadecane	C19H40	268	39.92
5	21.421	Silane, trichlorododecyl-	C22H45Cl3Si	442	75.82
6	22.257	trans-1-butyl-2-methylcyclopropane	C8H16	112	100.00
7	22.427	Di-n-octyl phthalate	C24H38O4	390	6.50
8	22.687	1-iodo-2-methylundecane	C12H25I	442	5.20
9	23.042	1-decanol, 2-methyl-	C11H24O	172	86.69
10	23.462	Hexyl octyl ether	C14H30O	214	5.24
11	23.797	cis-1-butyl-2-methylcyclopropane	C8H16	112	67.98
12	24.207	Octyl chloroformate	C9H17O2Cl	192	4.85
13	24.522	Dichloroacetic acid, nonyl ester	C11H20O2Cl2	254	46.45
14	25.238	Caproic acid, decyl ester	C11H21O2Cl	220	50.90
15	25.908	Oxirane, (1-methylbutyl)-	C7H14O	114	17.75
16	26.608	Methanamine, N-(1-methylbutylidene)-	C6H13N	99	17.50
17	27.389	N-Octane, 1-[1-cycloazapropyl]-	C10H21N	155	7.79
18	28.304	Azetidine, 1,2-dimethyl-	C5H11N	85	3.56
19	29.099	1,3,9-Cyclododecatriene, 1,5,9-trimethyl-	C15H24	204	4.34
20	29.444	Lupeol	C30H50O	426	8.14

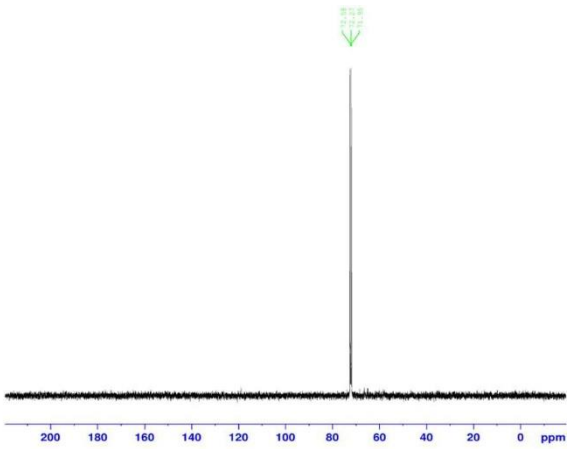

Fig 4.a. 13C NMR spectrum for water extract

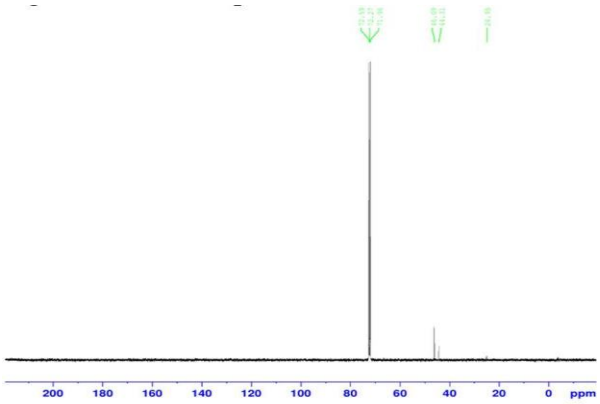

Fig 4.b. 13C NMR spectrum for methanolic extract

3.3 Computational studies

3.3.1. ADMET Properties

Phytoconstituent profiling from GC-MS expressed 25 bioactive compounds from both extracts, based on the parameters and their optimal ranges mentioned in previous section, ADMET properties are screened were from phytoconstituents only 12 molecules listed in Table 5 attain the maximum parameter ranges which will be further used as ligand molecules in docking studies.

3.3.2. Protein retrieval and preparation:

BMP proteins belonging to the TGF-β superfamily promote various activities that support bone health, from regular bone remodeling to fracture healing. BMP-2, BMP-3, BMP-6, BMP-7, and BMP-9 (Figure 5) are a few subtypes of BMP proteins, each with different activities. The PDB IDs of the retrieved protein structures were BMP-2: 2H64, BMP-3: 2QCQ, BMP-6: 2QCW, BMP-7: 1BMP, and BMP-9: 1ZKZ.

Table 5: Screened phytocompounds qualifying ADMET parameters

S. No.	Compound name	Molecular weight	Log P	Log S	Rotatable bonds	H	H-bond	G1	BBB (log)	Ames	Hep	Bioavailability	Skin
1	9-Hexadecenoic acid	254.41	5.3283	-5.477	13	1	1	92.51	0.084	NO	NO	0.85	YES
2	Silane, trichlorododecyl-	444.04	10.4656	-8.129	21	0	0	84.393	1.033	NO	NO	0.55	NO
3	Trans-1-butyl-2-methylcyclopropane	112.21	2.8326	-3.827	3	0	0	95.023	0.768	NO	NO	0.55	NO
4	Cis-1-butyl-2-methylcyclopropane	112.216	2.8326	-3.827	3	0	0	95.023	0.798	NO	NO	0.55	YES
5	1-Decanol, 2-methyl-	172.32	3.3604	-4.089	8	1	1	91.805	0.681	NO	NO	0.55	NO
6	Oxirane, (1-methylbutyl)-	114.19	1.8214	-1.638	3	1	1	97.375	0.64	NO	NO	0.55	YES
7	N-Octane, 1-[1-cycloazapropyl]-	155.28	2.6625	-3.008	7	1	0	91.754	0.68	NO	NO	0.55	YES
8	Azetidine, 1,2-dimethyl-	85.15	0.7104	-0.193	0	1	0	100	0.69	NO	NO	0.55	YES
9	Methanamine, N-(1-methylbutylidene)-	99.77	1.8772	-1.895	2	1	1	96.232	0.218	NO	NO	0.55	NO
10	Lupeol	426.72	8.0248	-8.0248	1	2	1	97.882	0.747	NO	NO	0.55	NO
11	4-Methylazolidine	87.12	-0.0478	-0.0478	0	1	1	100	-0.022	NO	NO	0.55	NO
12	Dichloroacetic acid, nonyl ester	255.85	4.0933	-4.0939	9	2	0	92.23	0.621	NO	NO	0.55	YES

Fig 5 : Structures of Bone Morphogenetic proteins (BMPs) subtypes

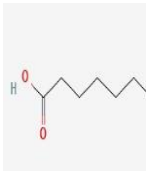

9-Hexadecenoic acid

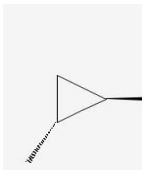

Trans-1-butyl-2-methylcyclopropane

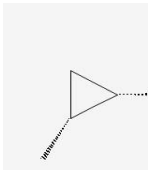

Cis-1-butyl-2-methylcyclopropane

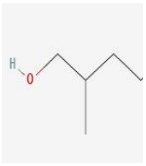

1-Decanol, 2-methyl-

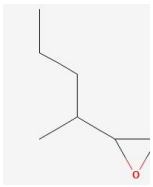

Oxirane (1-methylbutyl)-

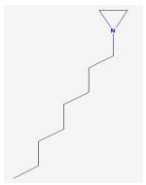

N-Octane 1-[1-cycloazapropyl]-

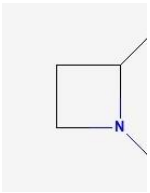

Azetidine, 1,2-dimethyl-

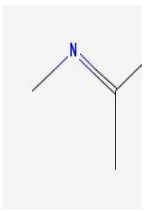

Methanamine, N-(1-methylbutylidene)-

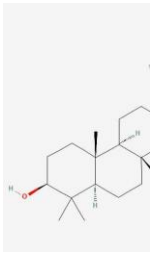

Lupeol

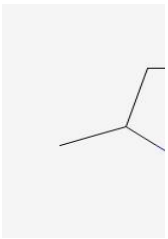

4-Methoxyazolidine

Dichloroacetic acid, nonyl ester

Fig 6 : 2D structures of Ligand molecules

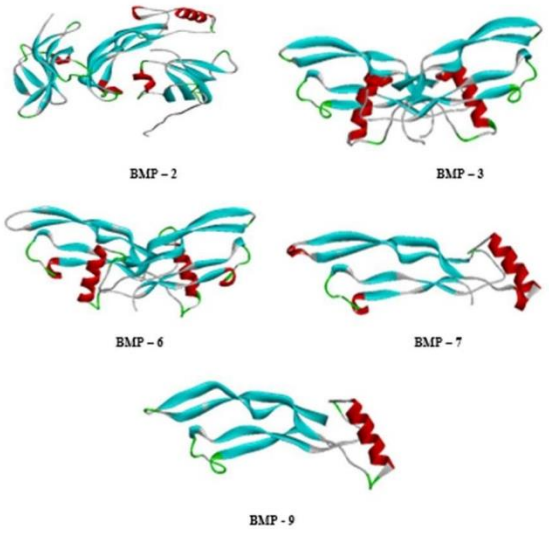

3.3.3. Ligand Retrieval and Preparation

The 12 phytocompounds were screened based on their ADMET parameters. Among the screened compounds, 11 phytocompounds were selected as ligand molecules for further molecular docking studies based on the availability of their three-dimensional (3D) structures. The selected ligand molecules were retrieved and prepared for docking analysis (Figure 6).

3.3.4. Molecular docking

Protein–ligand interaction analysis revealed multiple conventional hydrogen bonds and van der Waals interactions between phytoconstituents and BMP target proteins. BMP-2 interactions involved residues including His, Asp, Ser, Tyr, Phe, Gly, and Asn, while BMP-3, BMP-6, BMP-7, and BMP-9 demonstrated stable interactions with key amino acid residues contributing to ligand stabilization within the binding pocket. Among the screened compounds, 9-hexadecenoic acid and dichloroacetic acid nonyl ester exhibited notable binding affinities toward BMP-7 with docking scores of –5.2 and –4.8 kcal/mol, respectively. Several ligands, including trans-1-butyl-2-methylcyclopropane, cis-1-butyl-2-methylcyclopropane, and 1-decanol-2-methyl, demonstrated moderate binding affinities with BMP-6. Notably, Lupeol exhibited the strongest interaction across all targets, with docking scores of –8.0, –7.9, – 9.2, –7.5, and –7.0 kcal/mol against BMP-2, BMP-3, BMP-6, BMP-7, and BMP-9, respectively, indicating its potential osteogenic significance. Detailed interaction profiles and bond characteristics are presented in Table 6,7 and Fig. 8 series.

Table 6: Binding Affinity Score of Ligand–Protein Complexes

Sr. No.	Ligand	BMP-2	BMP-3	BMP-6	BMP-7	BMP-9
1	9-Hexadecenoic acid	-4.4	-4.6	-5.0	-5.2	-3.8
2	Trans-1-butyl-2-methylcyclopropane	-4.5	-4.1	-5.2	-4.8	-3.6
3	Cis-1-butyl-2-methylcyclopropane	-4.5	-4.0	-5.4	-4.8	-3.8
4	1-Decanol, 2-methyl-	-4.9	-4.4	-5.5	-4.8	-3.8
5	Oxirane (1-methylbutyl)-	-4.5	-3.7	-4.5	-4.0	-3.2
6	N-Octane 1-[1-cycloazapropyl]-	-4.3	-4.0	-5.3	-4.5	-3.5
7	Azetidine, 1,2-dimethyl-	-3.5	-3.3	-3.3	-3.2	-2.5
8	Methanamine, N-(1-methylbutylidene)-	-4.0	-3.7	-4.3	-3.9	-3.2
9	Lupeol	-8.0	-7.9	-9.2	-7.5	
10	4-Methoxyazolidine	-4.1	-3.2	-3.4	-3.2	
11	Dichloroacetic acid nonyl ester	-4.6	-4.3	-5.5	-4.8	

Table 7: Ligand interaction types and interacted amino acids in targeted proteins

		Bond type	BMP -2	BMP-3	BMP- 6	BMP-7	BMP-9
1	9-Hexadecanoic acid	Conventional H - Bond	B: His – 58, Tyr – 80, Ser – 83, Asp – 84	B: Asn – 53	A: Asp - 112	-	A: Gly - 108
		Unfavorable bump	HOH: B – 152, 172, 177,	-	A: HOH - 161	-	-

			188, 189 A - 212				
		Alkyl	Cys: B -87, 101 A: Trp - 31 Tyr - 91	A: Trp – 25, Phe – 87, Lys – 92, Tyr – 99	A: Phe – 40, Trp – 45, Ile – 49, Val – 107, Met – 124, Tyr – 169	A: Tyr – 116, Met – 131	A: Val – 15, Ile – 20, Trp – 22, Tyr – 32,
		Pi - sigma	-	-	A: Trp – 48, Tyr - 121	A: Trp – 52, 55; Tyr - 128	-
		Carbon H – Bond	-	-	-	A: Asp - 118	-
2	Trans-1-butyl-2-methylcyclopropane	Unfavorable bump	HOH: A – 135,143, 154,161,215 C - 101	-	A: HOH - 161	-	A: HOH - 144
		Alkyl	A: Pro - 35 Ile - 87 Val – 107	A: Trp – 22, Ile – 85, Met – 102 B: Ile - 85	A: Phe – 40, Trp – 45, 48; Ile – 49, Val – 107, Met – 124, Tyr-109, 121	A: Trp –52, Tyr – 116, 128	A: Trp – 25 Lys - 96
		Pi - sigma	-	A: Tyr - 99	-	A: Trp –55	A: Tyr – 86
3	Cis-1-butyl-2-methylcyclopropane	Unfavorable bump	HOH: A - 133,135, 143, 154, 161 C – 101	-	A: HOH - 161	-	A: HOH - 144
		Alkyl	Pro A – 35 Ile: A – 87 Val – 107	A: Trp – 22, Met - 102	A: Phe – 40, Trp – 45, 48; Ile – 49, Val - 107	A: Tyr – 116, 128	A: Lys – 96, Tyr - 99
		Pi - sigma	-	A: Tyr- 99	A: Tyr – 109, 121	A: Trp –52, 55	A: Trp – 25, 86
4	1-decanol, 2-methyl-	Conventional H - Bond	C: Asp – 62	-	-	A: Tyr - 128	A: Tyr – 35, Met – 102
		Carbon H- bond	-	-	B: Asn - 76	-	-
		Unfavorable bump	HOH - A - 133,135,143, 154, 161, 215; C – 101,110	-	A: Tyr - 109	-	-
		Alkyl	A: Pro – 35, His – 39, Ile – 87, Val - 107	A: Trp – 22, Ile - 85	A: Trp – 45, 48; Ile – 49, Val – 107, Met – 124, Tyr – 121	A: Trp – 52, 55	A: Val – 15, Ile – 20, Trp – 22, Ala – 34
		Water hydrogen bond	Asp: C - 62	-	-	-	-
		Pi - sigma	-	A: Trp – 25; Tyr- 99	A: Tyr - 109	-	-
5	Oxirane (1-	Conventional H -	A: His – 39	-	A: Trp - 48	-	A:

	methylbutyl)-	Bond					Asp – 47, 48
		Unfavorable bump	HOH: A – 133, 154, 161; C – 101	-	A: HOH - 161	-	-
		Alkyl	Pro: A- 35 Ile: A- 87	A: Trp – 25	A: Phe – 40, Trp – 45, Ile – 49, Val – 107, Tyr – 121, Met – 124	A: Trp – 52, Tyr - 116	A: Ala - 46
		Pi – sigma	-	A: Trp – 22, Tyr - 99	A: Tyr – 109	A: Trp - 55	-
6	N-octane 1-[1-cycloazapropyl]-	Carbon H - Bond	Asp: C - 62	-	-	A: Asp - 119	A: Tyr – 35, Gly - 101
		Unfavorable bump	HOH: A – 133, 135,143,154, 161, 215; C – 101,110	-	A: HOH – 161	-	-
		Alkyl	A: Pro - 35 Ile - 87 Val - 107	B: Trp – 22,25 Tyr - 99	A: Trp – 45, 48; Ile – 49, Val – 107, Tyr – 121, Met – 124	A: Trp – 55 Tyr – 116, 118	A: Val – 15, Ile – 20, Trp – 22, Ala - 34
		Pi – Sigma	-	-	A: Tyr - 109	A: Trp – 52	-
7	Azetidine 1,2-dimethyl-	Carbon H - Bond	C: Asp - 62	B: Asn - 53	-	-	A: Glu - 18
		Unfavorable bump	HOH: A – 133, 143,154, 161, 215; C – 101	-	A: HOH - 161		A: HOH – 133, 134
		Alkyl	A: Pro - 35 Ile - 87	A: Trp – 22, Ile-85 Met - 102	A: Trp - 45	-	A: Lys - 30
		Water hydrogen bond	HOH: A- 135; C – 110	-	-	-	-
		Pi- sigma	-	A: Tyr – 99	A: Tyr – 121		
		Van der Waals	-	-	A: Trp – 48, Ile – 49, Val – 107, Tyr - 109	-	-
8	Methanamine_n-(1-methylbutylidene)-	Carbon H - Bond	C: Asp - 62	-	-	A: Tyr - 116	-
		Unfavorable bump	HOH: A – 133, 143,154, 161; C – 101	-	A: HOH – 161	-	-
		Alkyl	A: Pro- 35 Ile- 87	A: Trp – 22, Tyr – 99 , Met -	A: Phe – 40, Ile – 49,	A: Trp – 52 Ile - 56	A: Leu – 13, Val – 15, Phe –

			102	Trp – 45, Val – 107		17, Trp – 22, Ala – 34, Met - 102
		Water hydrogen bond	HOH: A- 135;	-	-	-	-
		Conventional H - Bond	-	-	A: Tyr – 121	A: Tyr - 128	A: Tyr - 32
		Pi – sigma	-	-	-	A: Trp – 55	-
9	Lupeol	Conventional H - Bond	A: His - 39	-	-	-	-
		Unfavorable bump	HOH: A – 135, 143,193,215 C – 101,110, 122	HOH: B :124, 140; A – 121; Gly: A- 39	A: HOH – 161	-	A: HOH - 137
		Water H- bond	HOH: A- 154	-	-	-	-
		Alkyl	-	B: Ile - 3	A: Trp – 45, Ile – 49, Val – 107, Tyr – 109	-	A: Pro - 29
		Pi- sigma	-	-	A: Tyr - 121	-	-
10	4-methyloxazolidine	Conventional H - Bond	C: Asp – 63 Phe - 64	B: Arg – 110	A: Trp – 48, Tyr - 121	A: Pro - 59	A: Lys – 10, Cys – 107
		Unfavorable bond	HOH: A – 133, 154, 161; C - 101	A: HOH – 123	A: HOH - 161	-	A: HOH - 123
		Alkyl	A: Pro - 35 Ile - 87	A: Val – 76, Arg – 110 B: Val – 76	A: Trp – 45, Ile – 49, Val - 107	A: Phe – 56 Ile -56	-
		Water H- bond	-	A: HOH – 123	-	-	-
		Carbon H – bond	-	-	-	-	A: Cys - 8
11	Dichloroacetic acid nonyl ester	Conventional H - Bond	His: A- 39 Phe: C - 64	B: Thr – 56		A: Asp - 119	A: Tyr – 35, Val – 104
		Unfavorable bond	HOH: A- 135, 143, 215; C - 110	B: HOH – 111, 148	A: HOH- 161	-	-
		Alkyl	A: Ile - 87 Val - 107	A: Trp – 22, Ile – 85, Met – 102	A: Phe – 40, Trp :45, 48; Ile – 49, Val – 107, Tyr - 121	A: Trp – 52, 55, Tyr – 116, 128	A: Val – 15, Ile – 20, Trp – 22, Ala – 34,
		Water H - Bond	HOH: C - 101	-	-	-	-
		Van der Waals	-	A: Trp – 25, B: Asn – 53, Ile – 57, 60; Pro –44,51; Phe – 43, Met – 45	-	-	-

		Pi-Sigma	-	A: Tyr – 99	-	-	-
		Carbon H- Bond	-	-	-	-	A: Tyr – 32, Met – 102

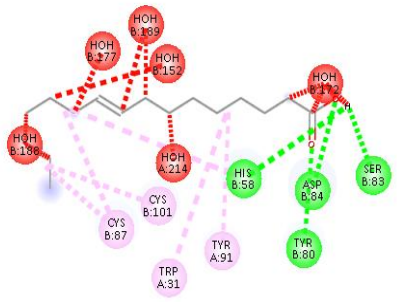

9-hexadecanoic acid

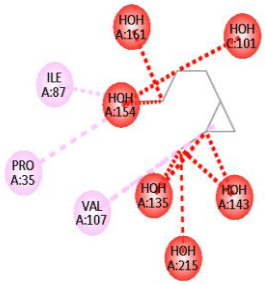

Trans-1-butyl-2-methylcyclopropane

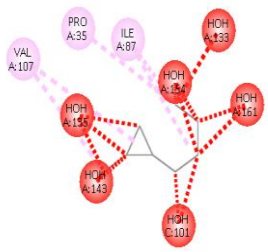

Cis-1-butyl-2-methylcyclopropane

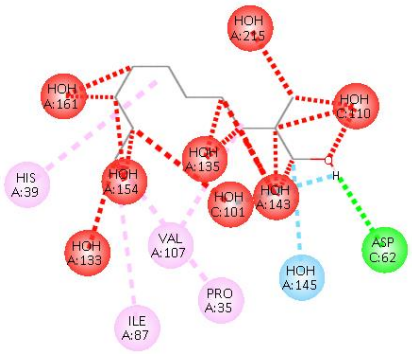

1-decanol_2-methyl-

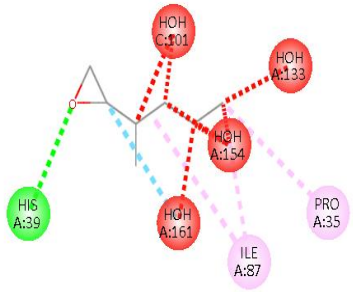

Oxirane, (1-methylbutyl)-

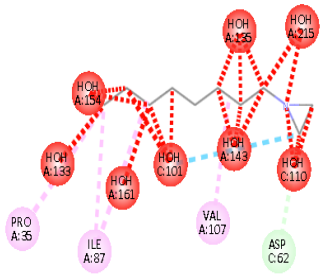

N-octane_1-[1-cycloazapropyl]-

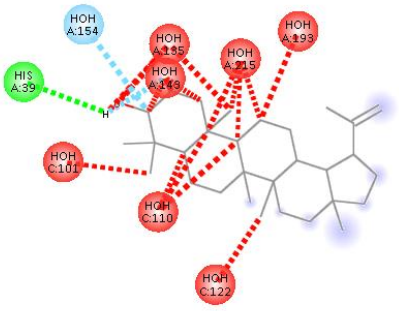

Lupeol

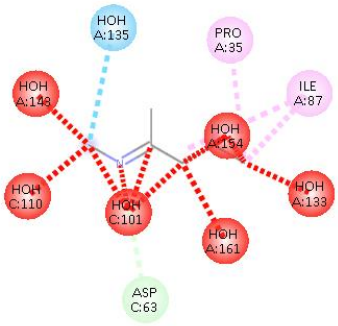

Methanamine_n-(1-methylbutylidene)-

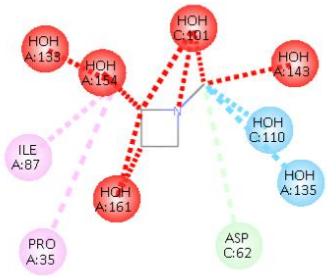

Azetidine,1,2-dimethyl-

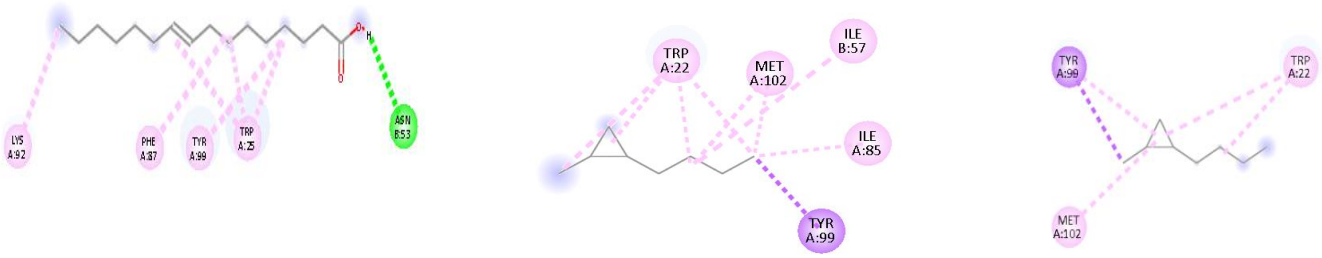

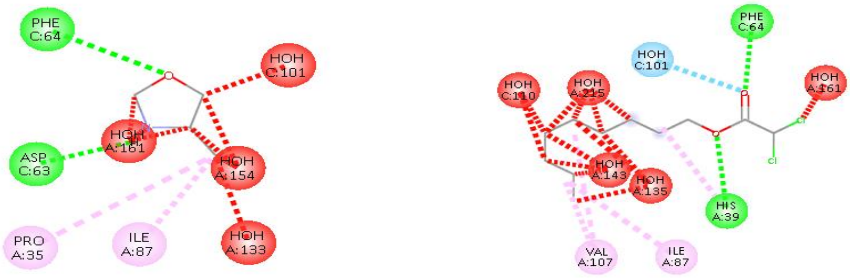

4-methyloxazolidine **Dichloroacetic_acid_nonyl_ester**

Fig 8.1. 2D diagrams of Ligand – protein interaction of BMP –2 target

3.3.4.2. BMP –3

9-hexadecanoic acid

Trans-1-butyl-2-methylcyclopropane

Cis-1-butyl-2-methylcyclopropane

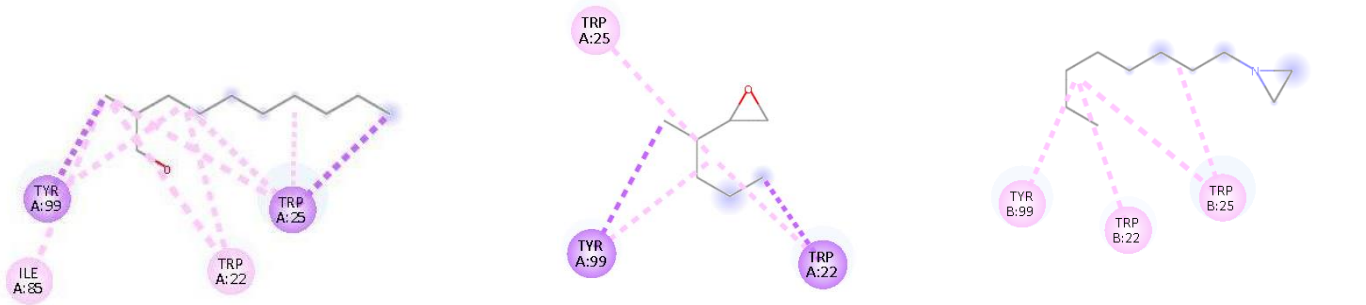

1-decanol 2-methyl-

Oxirane (1-methylbutyl)-

N-octane 1-[1-cycloazapropyl]-

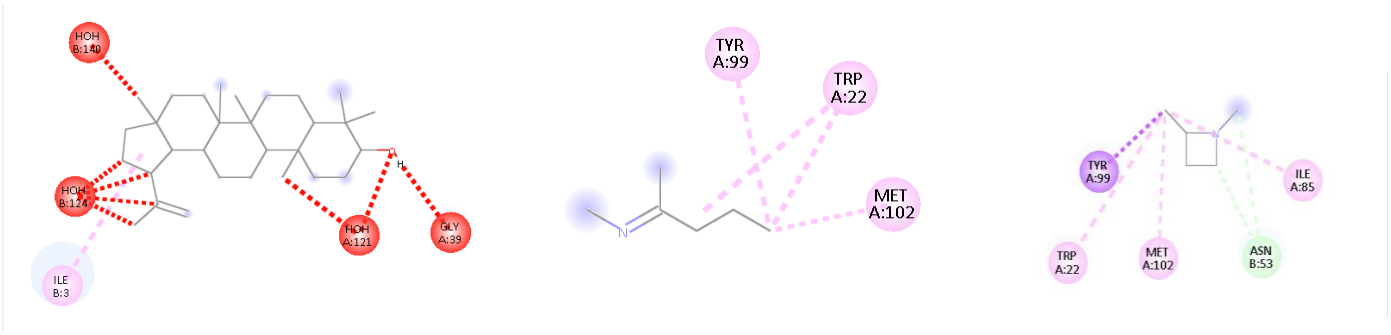

Lupeol

Methanamine_n-(1-methylbutylidene)-

Azetidine_1,2-dimethyl-

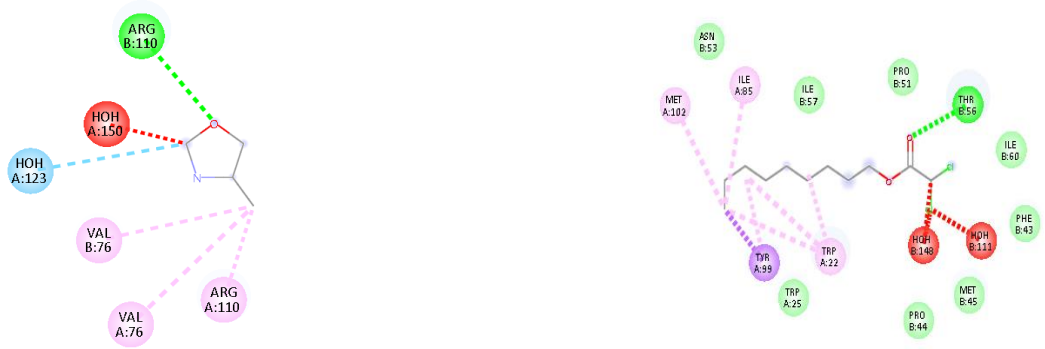

4-methyloxazolidine

Dichloroacetic_acid_nonyl_ester

Fig 8.2. 2D diagrams of Ligand – protein interaction of BMP –3 target

3.3.4.3. BMP –6

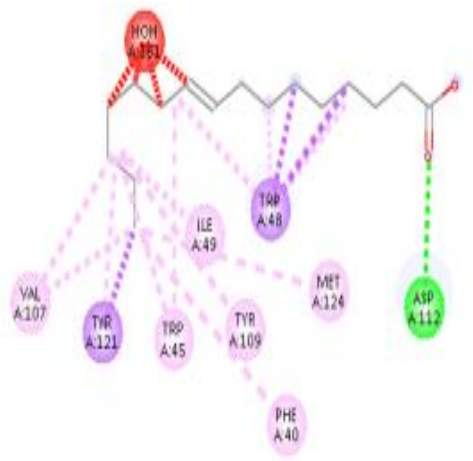

9-hexadecanoic acid

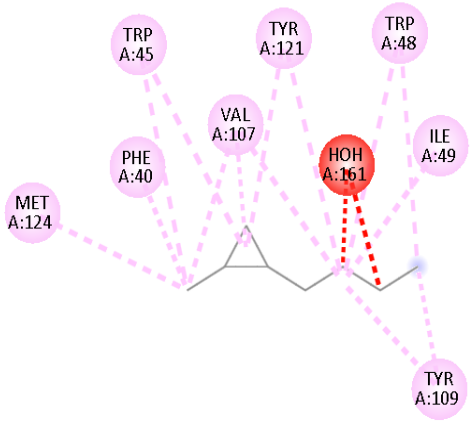

Trans-1-butyl-2-methylcyclopropane

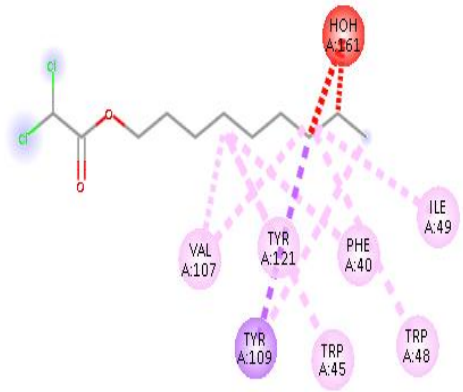

Cis-1-butyl-2-methylcyclopropane

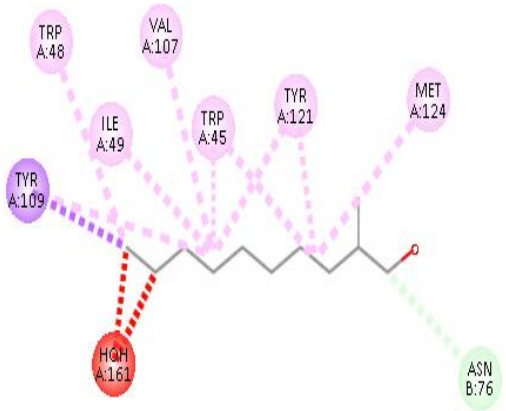

1-decanol, 2-methyl-

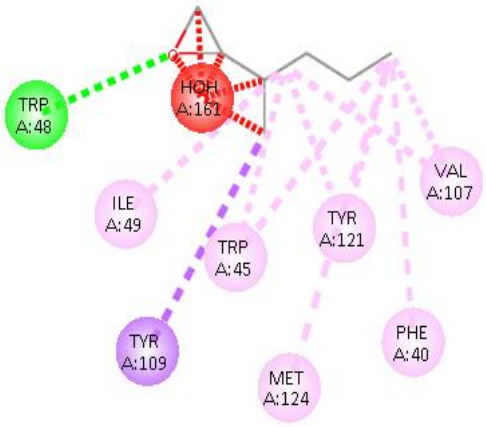

Oxirane(1-methylbutyl)-

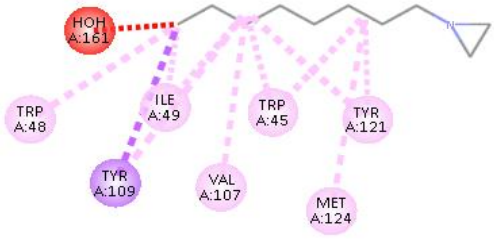

N-octane 1-[1-cycloazapropyl]-

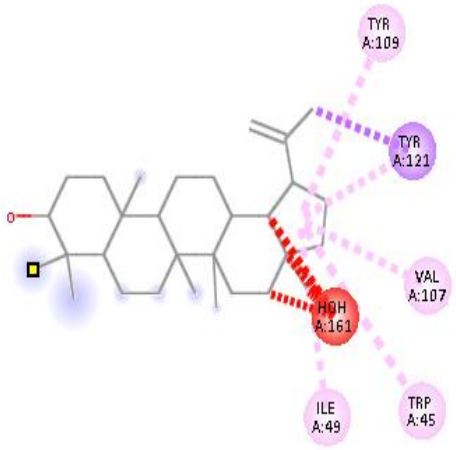

Lupeol

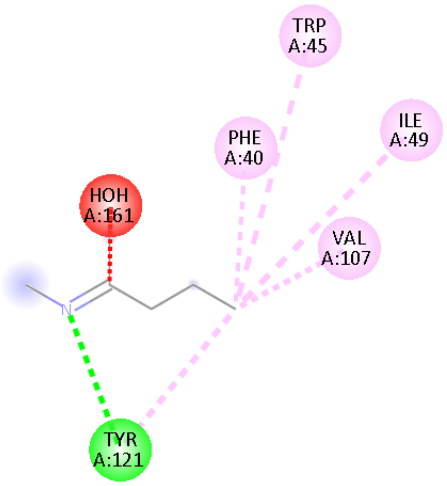

Methanamine n-(1-methylbutylidene)-

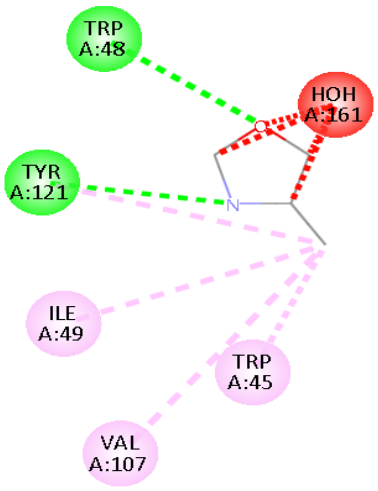

4-methyloxazolidine

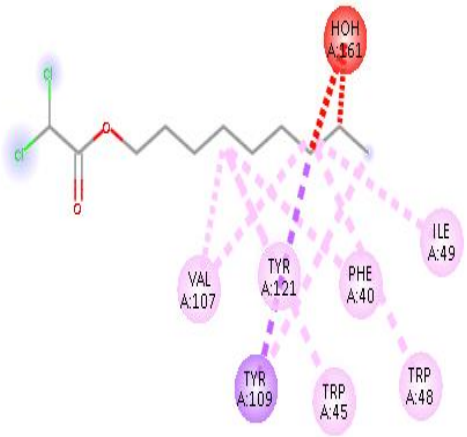

Dichloroacetic_acid_nonyl_ester

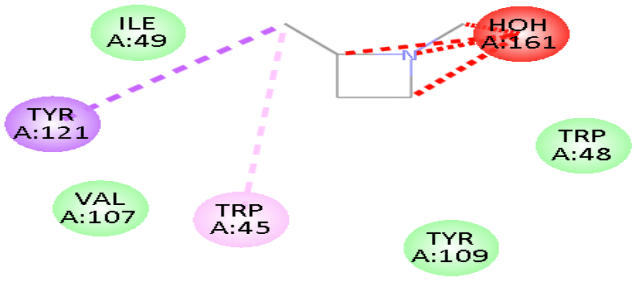

Azetidine 1,2-dimethyl-

Fig 8.3. 2D diagrams of Ligand – protein interaction of BMP –6 target

3.3.4.4. BMP –7

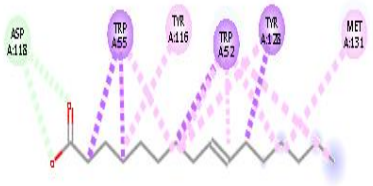

9-hexadecanoic acid

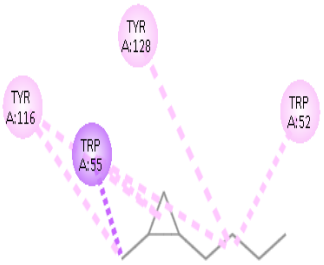

Trans-1-butyl-2-methylcyclopropane

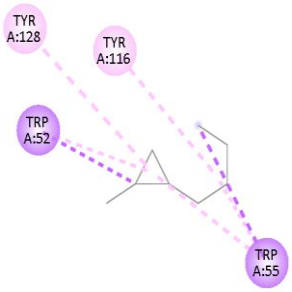

Cis-1-butyl-2-methylcyclopropane

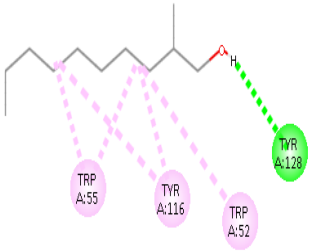

1-decanol_2-methyl-

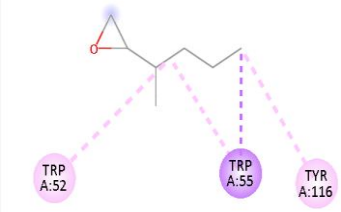

Oxirane_(1-methylbutyl)-

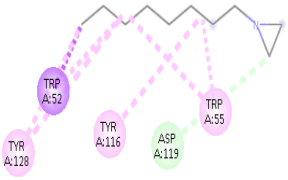

N-octane_1-[1-cycloazapropyl]-

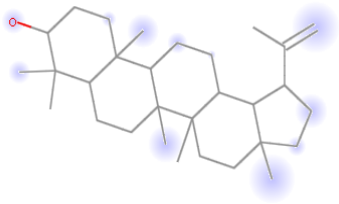

Lupeol

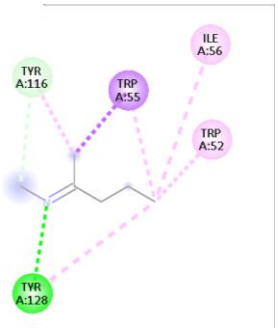

Methanamine_n-(1-methylbutylidene)-

Azetidine_1,2-dimethyl-

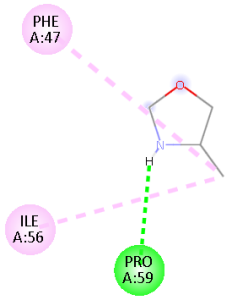

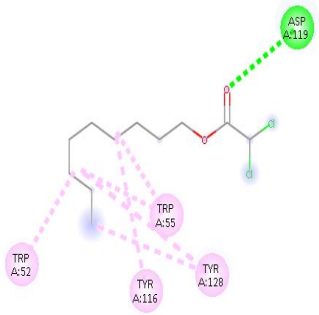

4-methyloxazolidine **Dichloroacetic_acid_nonyl_ester**

Fig 8.4. 2D diagrams of Ligand – protein interaction of BMP – 7 target

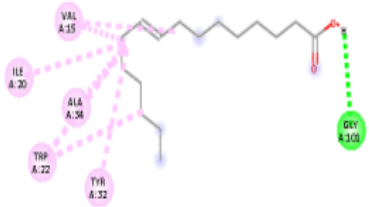

9-hexadecanoic acid

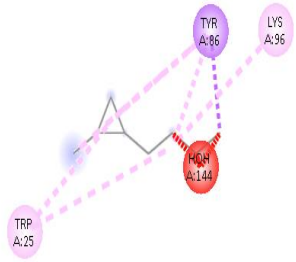

Trans-1-butyl-2-methylcyclopropane

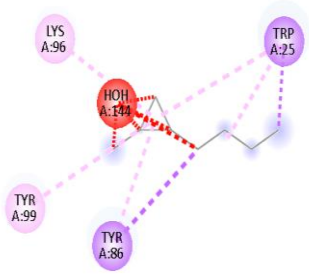

Cis-1-butyl-2-methylcyclopropane

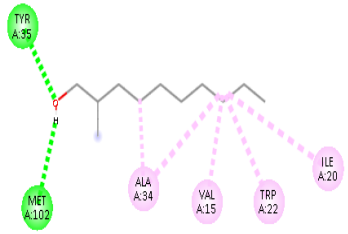

1-decanol_2-methyl-

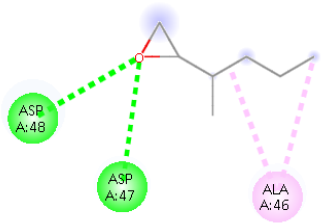

Oxirane_(1-methylbutyl)-

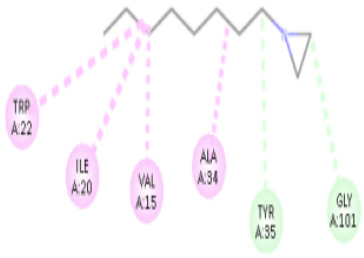

N-octane_1-[1-cycloazapropyl]-

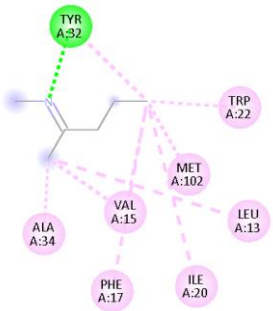

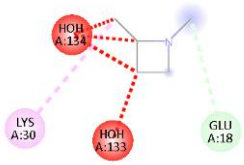

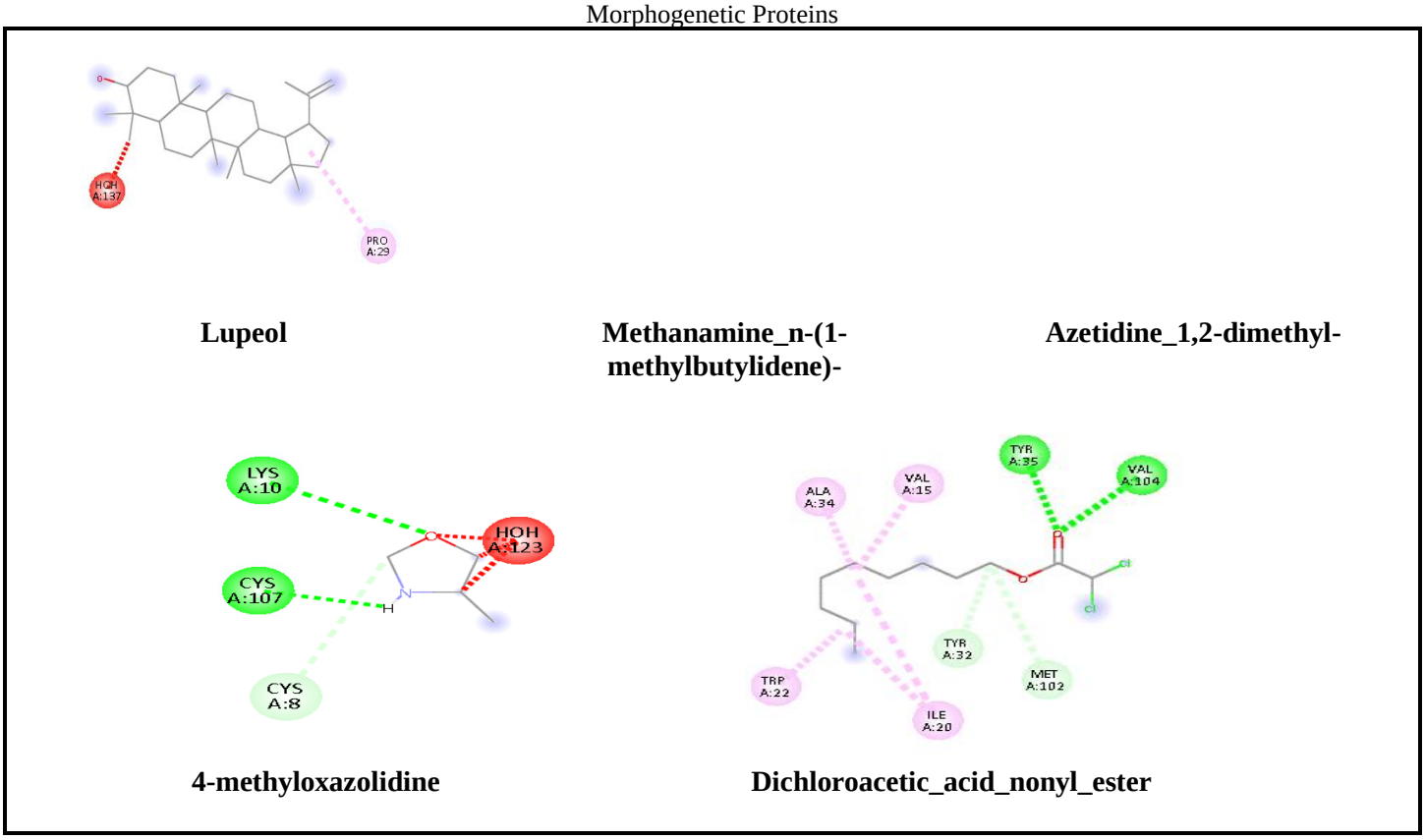

Fig 8.5. 2D diagrams of Ligand - protein interaction of BMP – 9 target

Azetidine 1,2-dimethyl-, 4-methyloxazolidine exhibited significant binding score with BMP 2, regulating the Smad Signaling pathway to activate osteoid. BMP-7 as like BMP-2 stimulates the collagen synthesis, deposition of calcium and mineralization by binding with 9-Hexadecanoic acid, Dichloroacetic acid nonyl. Whereas Trans-1-butyl-2-methylcyclopropane, Cis-1-butyl-2-

Conclusion

The present study investigated the phytochemical composition and in silico osteogenic potential of unripe fruit extracts of Diospyros malabarica. Phytochemical extraction was performed using methanol, n-hexane, and distilled water, with distilled water yielding the highest extract recovery (8.3%, w/w). Phytochemical characterization using FTIR, GC–MS, and NMR analyses revealed the presence of functional groups associated with bioactive compounds involved in osteogenic pathways. FTIR analysis of the n-hexane extract identified characteristic stretching vibrations of C–H, O–H, N–H, and C=O functional groups. GC–MS analysis revealed diverse classes of phytoconstituents, including lipids, hydrocarbons, epoxides, organosilicon compounds, terpenoids, triterpenoids, and alkaloids. Molecular docking studies were performed against Bone Morphogenetic Proteins (BMP-2, BMP-4, BMP-6, BMP-7, and BMP-9), which play essential roles in osteogenesis and bone remodeling. Among the screened compounds, lupeol exhibited the highest binding affinity with BMP-6 (–9.2 kcal/mol), indicating a potential interaction associated with osteogenic activity. The findings suggest that the n-hexane extract of *D. malabarica* contains phytoconstituents with potential osteogenic relevance, supporting its traditional medicinal application in bone-related disorders.(Kasmaei, L. S., Yasrebi, J., Zarei, M., Ronaghi, A., Ghasemi, R., Saharkhiz, M. J., ... & Schnug 2019)

REFERENCES:

Kasmaei, L. S., Yasrebi, J., Zarei, M., Ronaghi, A., Ghasemi, R., Saharkhiz, M. J., ... & Schnug, E. 2019. "Detection and Molecular Analysis of Hop Latent Virus and Hop Latent Viroid in Hop Samples from Poland Originalarbeit." *JOURNAL FÜR KULTURPFLANZEN* 66(7). doi: 10.5073/J.

1. *Chemical Constituents of the Fruit Essential Oil of Diospyros Malabarica (Desr.) Kostel (Ebenaceae)*;
2. Kavatagimath, S.A.; Jalalpure, S.S. Screening of Ethanolic Extract of Diospyros Malabarica Desr. Bark for Anti-Diabetic and Antioxidant Potential. *Indian Journal of Pharmaceutical Education and Research* **2016**, *50*, 179–189, doi:10.5530/ijper.50.1.223
3. Rode, M.S.; Kalaskar, M.G.; Gond, N.Y.; Surana, S.J. Evaluation of Anti-Diarrheal Activity of Diospyros Malabarica Bark Extract. *Bangladesh J Pharmacol* **2013**, *8*, 49–53, doi:10.3329/bjp.v8i1.13157.
4. Baidya, S.; Devi, A. *ROLE OF INDIGENOUS COMMUNITIES IN CONSERVATION OF SACRED PLANTS OF ASSAM*; 2018;
5. Shrestha, R.; Dawadi, P.; Bhusal, S.; Bhatt, L.R. Nutritional Value and Antioxidant Properties of Diospyros Malabarica (Desr.) Kostel., Fruit from Midhills of Western Nepal. *Nepal J Sci Technol* **2021**, *20*, 113–125, doi:10.3126/njst.v20i1.43361.
6. Siddique, H. *Bangladeshi Medicinal Plants: Ethnopharmacology, Phytochemistry and Anti-Staphylococcal Activity*; 2019;
7. Azeemi, S.K.; Khan, Z.-U.-D.; Shazia, *; Malik[1], K.; Khan[2], Z.-U.-D.; Khan[3], F. *Investigation of In-Vitro Anthelmintic Potential of Fruits of Some Ethnobotanically Important Trees of Punjab, Pakistan*; 2015;
8. S Rajamanoharan, P.R.; Pholtan Rajeev, S.R. EXISTENCE AND SURVEY OF MEDICINAL PLANTS OF THIRU PALANI MURUGAN KOVIL, ASIKULAM, VAVUNIYA DISTRICT, NORTHERN PROVINCE, SRI LANKA. *Rajeev. World Journal of Pharmaceutical Research* **2016**, *5*, doi:10.20959/wjpr201611-6702.
9. Kaushik, V.; Niketan, S.; Saini, V.; Pandurangan, A.; Lal Khosa, R.; Parcha, V. *A Review of Phytochemical and Biological Studies of Diospyros Malabarica*; 2013; Vol. 2;
10. Sharmin, T.; Sultana, R.; Hossain, F.; Shakil, S.K.; Hossen, F.; Rashid, Md.M.O. Neuropharmacological and Antibacterial Effects of the Ethyl Acetate Extract of Diospyros Malabarica (Ebenaceae) Seeds. *Clinical Phytoscience* **2018**, *4*, doi:10.1186/s40816-018-0083-x.
11. Kavatagimath, S.A.; Jalalpure, S.S. Screening of Ethanolic Extract of Diospyros Malabarica Desr. Bark for Anti-Diabetic and Antioxidant Potential. *Indian Journal of Pharmaceutical Education and Research* **2016**, *50*, 179–189, doi:10.5530/ijper.50.1.22

Abegunasekara, N.S.; Bandara, A.M.A.G.K.S. Comparative Study of Coagulation Effect of Diospyros Malabarica. *INTERNATIONAL JOURNAL OF APPLIED PHARMACEUTICAL SCIENCES AND RESEARCH* **2019**, *4*, 43–49, doi:10.21477/ijapsr.4.3.2.

12. Chowdhury, M.; Sultana, L.A.; Joya, A.C.; Shomudro, H.K. Pharmacological Investigation of In-Vitro Anti-Inflammatory, Antimicrobial, Thrombolytic, Cytotoxic and In Vivo Analgesic Activities of Ethanolic Leaf Extract of Diospyros Malabarica. *J Adv Med Pharm Sci* **2023**, *25*, 1–11, doi:10.9734/jamps/2023/v25i8630.
13. Javed, S.; Rehman, S.; Zaman Khan, M.; Khalid, A.; Qaseem, R.; Humayun, M. *EVALUATION OF IN VITRO PHARMACOLOGICAL ACTIVITIES OF DIOSPYROS MALABARICA KOSTEL FRUIT*;
14. Azeemi, S.K.; Khan, Z.-U.-D. *EVALUATION OF THE BIOLOGICAL ACTIVITIES OF FRUIT OF Diospyros Malabrica (KOSTEL)*; 2019;
15. Liu, H.; Li, D.; Zhang, Y.; Li, M. Inflammation, Mesenchymal Stem Cells and Bone Regeneration. *Histochem Cell Biol* 2018, *149*, 393–404.
16. Mohammed, M.S.; Osman, W.J.A.; Garelnabi, E.A.E.; Osman, Z.; Osman, B.; Khalid, H.S.; Mohamed, M.A.; Osman, J.A. *Secondary Metabolites as Anti-Inflammatory Agents*; 2014; Vol. 3;.
17. Hariyanto, N.A.; Ramadhan, R.; Raharjo, Y.; Firdaus, Y.F.H.; Kurnia, I.T.; Lestari, D.A.; Suwandari, S.; Mahmuda, N.F.; Nathanael, J.; Phontree, K.; et al. GC-MS Analysis of Three Diospyros Species and Evaluation of Its in Vitro Rat Intestinal α-Glucosidase and FRAP Activity. *Biodiversitas* **2024**, *25*, 2442–2453, doi:10.13057/biodiv/d250613.
18. Ralston, S.H. *Bone Structure and Metabolism*;
19. Boskey, A.L.; Robey, P.G. *6 The Composition of Bone*; 2013;
20. Fazzalari, N.L. Bone Fracture and Bone Fracture Repair. In Proceedings of the Osteoporosis International; June 2011; Vol. 22, pp. 2003–2006.

21. Elnawary, H.; Baradaran, A.; Abi-Rafeh, J.; Vorstenbosch, J.; Xu, L.; Efanov, J.I. Bone Healing and Inflammation: Principles of Fracture and Repair. *Semin Plast Surg* **2021**, *35*, 198–203, doi:10.1055/s-0041-1732334.
22. Arvidson, K.; Abdallah, B.M.; Applegate, L.A.; Baldini, N.; Cenni, E.; Gomez-Barrena,
23. Hanga-Farcaș, A.; Miere, F.; Filip, G.A.; Clichici, S.; Fritea, L.; Vicaș, L.G.; Marian, E.; Pallag, A.; Jurca, T.; Filip, S.M.; et al. Phytochemical Compounds Involved in the Bone Regeneration Process and Their Innovative Administration: A Systematic Review. *Plants* 2023, *12*.
24. Katagiri, T.; Watabe, T. Bone Morphogenetic Proteins. *Cold Spring Harb Perspect Biol* **2016**, *8*, doi:10.1101/cshperspect. a021899.
25. Hayrapetyan, A.; Jansen, J.A.; Van Den Beucken, J.J.J.P. Signaling Pathways Involved in Osteogenesis and Their Application for Bone Regenerative Medicine. *Tissue Eng Part B Rev* **2015**, *21*, 75–87, doi: 10.1089/ten.teb.2014.0119.
26. Yang, J.; Shi, P.; Tu, M.; Wang, Y.; Liu, M.; Fan, F.; Du, M. Bone Morphogenetic Proteins: Relationship between Molecular Structure and Their Osteogenic Activity. *Food Science and Human Wellness* **2014**, *3*, 127–135, doi: 10.1016/j.fshw.2014.12.002.
27. Agarwal, S.; Mehrotra, R. An Overview of Molecular Docking. *JSM Chem* **2016**, *4*, 1024.
28. Himi, A.S.; Pramanik, M.; Kubra, K.; Muntaher, M.; Anika, K.A.; Islam, Md.A.; Mia, Md.S. Phytochemical & Pharmacological Activities of Diospyros Malabarica. *European J Med Plants* **2025**, *36*, 43–60, doi:10.9734/ejmp/2025/v36i21246.
29. Zreen, Z.; Hameed, A.; Kiran, S.; Farooq, T.; Zaroog, M.S. A Comparative Study of Diospyros Malabarica (Gaub) Extracts in Various Polarity-Dependent Solvents for Evaluation of Phytoconstituents and Biological Activities. *Biomed Res Int* **2022**, *2022*, doi:10.1155/2022/4746223.
30. FTIR Functional Group Database Table with Search - InstaNANO. Https://Instanano.Com/All/Characterization/F tir/Ftir-Functional-Group-Search/ (Accessed April 2nd, 2025).
31. Infrared_Spectroscopy_Absorption_Table.
32. Specht, T.; Münnemann, K.; Hasse, H.; Jirasek, F. Automated Methods for Identification and Quantification of Structural Groups from Nuclear Magnetic Resonance Spectra Using Support Vector Classification. *J Chem Inf Model* **2021**, *61*, 143–155, doi:10.1021/acs.jcim.0c01186.
33. Falcigno, L., D'Auria, G., Calvanese, L., Marasco, D., Iacobelli, R., Scognamiglio, P. L., ... & Dettin, M. (2015). Osteogenic properties of a short BMP-2 chimera peptide. *Journal of Peptide Science*, *21*(9), 700-709.
34. Cecilia, P. H., Nugraha, A. P., Shariff, K. A., Kharisma, V. D., Ramadhani, N. F., Sitalaksmi, R. M., ... & Narmada, I. B. (2024). Molecular docking of beta tricalcium phosphate combined with dicalcium

35.

Journal of International Dental and Medical Research, *17*(2), 470-479.

36.